

# TRACKING CHANGES IN FUNCTIONAL CONNECTIVITY OF BRAIN NETWORKS FROM RESTING-STATE FMRI USING PARTICLE FILTERS

*M Faizan Ahmad<sup>a</sup>, James Murphy<sup>a</sup>, Deniz Vatansever<sup>b</sup>, Emmanuel A Stamatakis<sup>b</sup>, Simon Godsill<sup>a</sup>*

<sup>a</sup>Department of Engineering, University of Cambridge, UK

<sup>b</sup>Department of Clinical Neurosciences, Addenbrooke's Hospital, Cambridge, UK

## ABSTRACT

Recent empirical research has discovered that linkages among fMRI signals of the brain in resting-state have meaningful temporal variations. Most current studies of brain networks assume that these linkages are constant. We propose a model and an accompanying algorithm to infer and track changes in these interaction strengths, thus providing a more comprehensive way to study brain dynamics. The stochastic model employed is akin to one used for neuronal states (DCM) and a Rao-Blackwellized filtering algorithm is set up for tracking purposes. Our results show that time-varying interactions among brain regions can be successfully found which have the potential of providing great clinical value.

**Index Terms**— resting state fMRI, functional connectivity, BOLD, Rao-Blackwellized particle filter.

## 1. INTRODUCTION

Brain research has shifted its focus from studying segregation of the brain into discrete parts to attempting to discern the integration among its different interacting components. Whereas several imaging modalities are available such as PET (positron emission tomography), EEG and MEG (electro and magneto encephalography), fMRI (functional magnetic resonance imaging) is the dominant approach as it is non-invasive, efficient, cost-effective and offers superior spatial resolution. The measured fMRI signal is the result of the BOLD (blood oxygenation level dependent) effect and reflects an increased local demand for oxygen in brain regions with elevated neural activity. Functional connectivity is widely quantified using temporal correlation among BOLD signals[1][2][3], Mutual

Information[4][5] or Independent Component Analysis[6]. These strategies give time-averaged results over the observed data, hence capturing no temporal variation and greatly simplifying the analysis. More complex and biologically meaningful models exist that describe the interaction between neuronal regions and relate these to the resultant hemodynamic response measured implicitly by fMRI. These include structural equation modelling (SEM)[7] and deterministic and stochastic dynamic causal modelling (DCM)[8][9][10][11]. Though schemes such as Dynamic Expectation Maximisation[12], Variational Bayes[13], Metropolis-Hastings[14] and Particle Filtering[15] have been used to track hidden states and estimate (constant) physiological parameters, they do not account for time-varying dependencies between different regions of the brain.

Recent evidence suggests that dynamic functional connectivity exhibited by BOLD signals may have a neuronal origin [16][17]. It is thus worthwhile to study the time-varying nature of these networks as they could yield better insight into brain functions as well as having potential clinical value by providing disease markers for diagnostic purposes. The few instances in the literature that address temporal features are largely limited to sliding window approaches[16][18][19][20] which have numerous limitations including high sensitivity to noise and choice of window size.

Functional networks in resting state fMRI, which occur when there is no external input and which persist even during sleep and anesthesia, have been identified as being similar to those in task focused fMRI, and have been used to draw fundamental mapping of the brain[21]. It is believed that during the time period in which data acquisition occurs, the brain would not be in a resting state all the time but would go into 'active' episodes, thus undergoing a dynamic response[22]. The aim of this paper is to identify this transient response and distinguish subsequent networks formed by identifying changes in inter-regional interaction.

This paper comprises five sections. Section 2 presents a dynamic model where the states of different brain regions are dependent on other nodes through smoothly time-

---

This work was supported by the Engineering and Physical Sciences Research Council (EPSRC) grant number EP/K020153/1 and Yousef Jameel Scholarship Programme.

varying linkage parameters. It then explains a marginalized particle filtering algorithm to compute estimates for these dynamic parameters describing changes in the underlying network. The methodology is first verified on synthetic data in Section 3 before it is tested on real data of resting state fMRI in Section 4. Conclusions and suggestions for future work are discussed in Section 5.

## 2. METHODOLOGY

### 2.1. Model

BOLD signals  $x_{i,t}$  at each node (brain location) are modelled as being linked to those at all other nodes (including themselves) via the following linkage model, in which the effect of node  $j$  on node  $i$  depends on the  $\varphi_{i,j,t}$  parameter

$$d\dot{x}_{i,t} = \sum_{j=1}^N \varphi_{i,j,t} x_{j,t} dt + dW_{i,t}, \quad (1)$$

where  $x_{i,t}$  is magnitude of the BOLD signal at node  $i$  at time  $t$  and  $\dot{x}_{i,t}$  is its rate of change;

$\varphi_{i,j,t}$  is the interaction parameter between nodes  $i$  and  $j$  at time  $t$ ;

$W_{i,t}$  is random noise generated independently for node  $i$ ;

$N$  is the total number of nodes in the network.

The system can be described as a linear stochastic differential equation of the form

$$dX_t = A_t X_t dt + B dW_t, \quad (2)$$

where  $X_t \in R^{2N \times 1}$  is  $[x_{t,1}, \dot{x}_{t,1}, x_{t,2}, \dot{x}_{t,2}, \dots, x_{t,N}, \dot{x}_{t,N}]^T$  and is the state of all nodes (magnitude and rate of change) at time  $t$ .

The matrix  $A_t \in R^{2N \times 2N}$  is defined as:

$$A_t = \begin{bmatrix} 0 & 1 & 0 & \dots \\ \varphi_{1,1,t} & 0 & \varphi_{1,2,t} & 0 & \varphi_{1,3,t} & \dots & \dots & \dots & \dots & \dots \\ 0 & 0 & 0 & 1 & 0 & \dots & \dots & \dots & \dots & \dots \\ \varphi_{2,1,t} & 0 & \varphi_{2,2,t} & 0 & \varphi_{2,3,t} & \dots & \dots & \dots & \dots & \dots \\ & & & & & & & & & & \vdots \\ & & & & & & & & & & \vdots \\ & & & & & & & & & & \vdots \end{bmatrix} \quad (3)$$

and  $B \in R^{2N \times N}$  is given by

$$B = \begin{bmatrix} B_1 & \dots & 0 \\ \vdots & \ddots & \vdots \\ 0 & \dots & B_1 \end{bmatrix}; B_1 = \begin{bmatrix} 0 \\ 1 \end{bmatrix}. \quad (4)$$

The observation model is specified as

$$z_{i,t} = x_{i,t} + v_{i,t}, \quad (5)$$

where  $v_t$  is random noise having a Gaussian distribution with a mean of zero and variance  $\sigma_z^2$  and the state equation is analogous to stochastic DCM for neurological networks used for resting-state data (i.e. not involving any exogenous inputs)[23]. The noise term in Equation (2) represents physiological noise such as cardiac motion, variation in

respiratory volume etc. whereas that in Equation (5) models measurement noise. This model allows the problem to be cast in probabilistic terms. In order to estimate the BOLD signals  $X_t$  and their linkages  $\varphi_{i,j,t}$  from observations, the aim is to calculate the posterior probability distribution  $p(X_t, \phi_t | Z_{1:t})$  where  $\phi_t \in R^{M \times 1}$  is  $[\varphi_{1,1,t}, \varphi_{1,2,t}, \dots, \varphi_{N,N,t}]^T$ ,  $Z_t \in R^{N \times 1}$  is  $[z_{1,t}, z_{2,t}, \dots, z_{N,t}]^T$  and  $Z_{1:t}$  is the observation set up to time  $t$ .

The transition probability from one time period to the next for  $X_t$  and  $\phi_t$  is modelled as

$$p(X_t, \phi_t | X_{t-1}, \phi_{t-1}) = p(\phi_t | \phi_{t-1}) p(X_t | X_{t-1}, \phi_t), \quad (6)$$

where  $\phi_t$  depends on  $\phi_{t-1}$  only and  $X_t$  depends on the previous state  $X_{t-1}$  and the current values of  $\phi$  variables. Interaction parameters are allowed to vary with time according to the following model (i.e. a random walk prior)

$$p(\phi_t | \phi_{t-1}) = \mathcal{N}(\phi_t | \phi_{t-1}, \sigma_\phi^2 I), \quad (7)$$

$$p(X_t | X_{t-1}, \phi_t) = \mathcal{N}(X_t | F_t(\phi_t) X_{t-1}, Q_t(\phi_t)), \quad (8)$$

where  $I$  is an identity matrix. The transition matrix  $F_t$  and covariance matrix  $Q_t$  depend on the interaction parameters  $\phi_t$  and are found according to calculations given in [24]. The observation probability density for the joint state is given by:

$$p(Z_t | X_t) = \mathcal{N}(Z_t | H X_t, \sigma_z^2 I), \quad (9)$$

where  $H \in R^{N \times 2N}$  is defined as

$$H = \begin{bmatrix} H_1 & \dots & 0 \\ \vdots & \ddots & \vdots \\ 0 & \dots & H_1 \end{bmatrix}; H_1 = [1 \quad 0]. \quad (10)$$

### 2.2. Algorithm

Instead of using a generic bootstrap particle filter which does not handle a large number of variables adequately, a marginalized filter is set up using a procedure known as Rao-Blackwellization, followed by particle smoothing [25]. It can be seen from the model equations that the overall state can be partitioned into two components: signal magnitudes and their rates of change:  $X_t$ , and linkage parameters:  $\phi_t$ . Conditional upon the linkage parameters, the signals and rates are linear and Gaussian, thus standard linear Gaussian optimal filtering (Kalman filtering) may be used to infer them. Particle filtering can be used to infer the distribution of the nonlinear  $\phi_t$  portion of the state, which is approximated as a weighted collection of samples  $\phi_t^{(i)}$  with  $i = 1, \dots, M$ .

Conditional on each sample of  $\phi_t^{(i)}$  in the particle collection, the linear part  $X_t$  is expressed in the form of a linear Gaussian state-space model as follows:

$$X_t = F_t(\phi_t^{(i)})X_{t-1} + u_t, \quad (11)$$

$$Z_t = HX_t + v_t. \quad (12)$$

Noise is represented by terms  $u_t$  and  $v_t$  which are independent, zero-mean and Gaussian, with covariance matrices given by  $C_u = Q_t(\phi_t^{(i)})$  and  $C_v = \sigma_z^2 I$ . The parameters  $\phi_t^{(i)}$  are sampled for each  $i$ -th particle according to the first-order Markov chain model given in Equation (7). Then, for each particle, conditioned on  $\phi_t^{(i)}$  and observations  $Z_{0:t}$ , the linear part  $X_t$  can be calculated using Kalman filtering on the system. Since the distribution of  $X_t$  found via Kalman filtering is Gaussian, the posterior over  $X_t$  is a weighted Gaussian mixture model, with one component corresponding to each particle.

Conditioned on each sample  $\phi_t^{(i)}$ , the predictive distribution of  $X_t$  conditioned upon all past measurements is given by

$$p(X_t | Z_{1:t-1}, \phi_{1:t}^{(i)}) = \mathcal{N}(X_t | \mu_{t|1:t-1}, C_{t|1:t-1}), \quad (13)$$

where

$$\mu_{t|1:t-1} = F_t(\phi_t)\mu_{t-1|1:t-1}, \quad (14)$$

$$C_{t|1:t-1} = F_t(\phi_t)C_{t-1|1:t-1}(F_t(\phi_t))^T + C_u. \quad (15)$$

After obtaining the current measurement  $Z_t$ , the posterior distribution of  $X_t$  is given by

$$p(X_t | Z_{1:t}, \phi_{1:t}^{(i)}) = \mathcal{N}(X_t | \mu_{t|1:t}, C_{t|1:t}), \quad (16)$$

where

$$\mu_{t|1:t} = \mu_{t|1:t-1} + K_t(Z_t - H\mu_{t|1:t-1}), \quad (17)$$

$$C_{t|1:t} = (I - K_t H)C_{t|1:t-1}, \quad (18)$$

$$K_t = C_{t|1:t-1}H^T(HC_{t|1:t-1}H^T + C_v)^{-1}. \quad (19)$$

Since the posterior distribution of  $X_t$  found via this Kalman filtering is Gaussian, the posterior over  $X_t$  is a weighted Gaussian mixture model, with one component corresponding to each particle.

The following term can also be computed using the prediction error

$$p(Z_t | Z_{1:t-1}, \phi_{1:t}) = \mathcal{N}(Z_t | \mu_{Z_t}, C_{Z_t}), \quad (20)$$

where

$$\mu_{Z_t} = H\mu_{t|1:t-1}, \quad (21)$$

$$C_{Z_t} = HC_{t|1:t-1}H^T + C_v. \quad (22)$$

This can be used to update the weight of each particle according to

$$\tilde{\omega}_t^{(i)} = \omega_{t-1}^{(i)} p(Z_t | Z_{1:t-1}, \tilde{\phi}_t^{(i)}), \quad (23)$$

where initially  $\omega_o^{(i)} = 1/N$  for all  $i$ . The posterior distribution of the interaction parameters is approximated by the weighted particle collection as:

$$p(\phi_t | Z_{1:t}) \approx \sum_i \tilde{\omega}_t^{(i)} \delta(\tilde{\phi}_t^{(i)}). \quad (24)$$

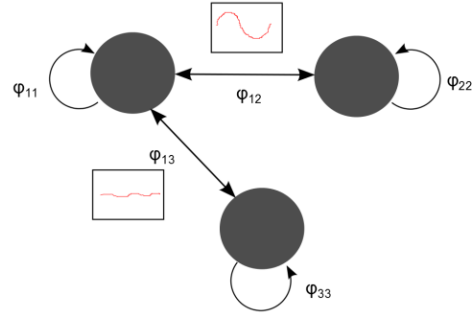


Figure 1: Simulated network diagram

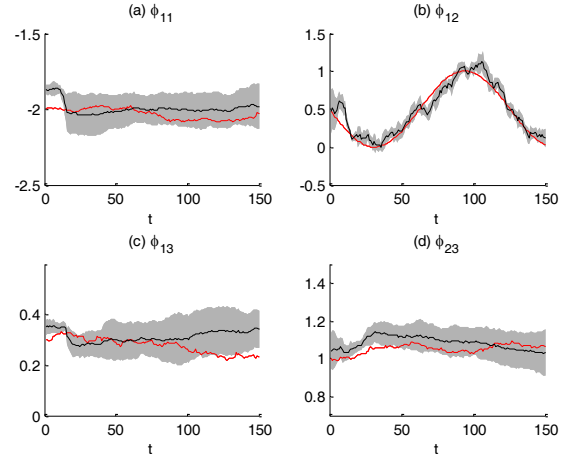


Figure 2: Tracking results from synthetic data. Red line shows true value. Black line shows estimated mean and grey region shows 1 standard deviation

Table 1: Comparison of RMSE obtained from sliding window approach and particle filtering

Average RMSE	Sliding Window	Particle Filtering
$N = 2$	0.270	0.187
$N = 3$	0.296	0.207
$N = 4$	0.408	0.142
$N = 5$	0.431	0.250
$N = 6$	0.409	0.325

### 3. SIMULATED DATA

Due to lack of ground truth available from experimental data, the algorithm is first tested on a synthetic sample in order to verify its robustness and efficiency, and confirm its ability to estimate meaningful results when applied to experimental fMRI data. A symmetric three-node network is considered with a sinusoidally varying link, a nearly constant link and a non-existent link as shown in Figure 1.

Results depicted in Figure 2 demonstrate that our algorithm tracks both the varying and nearly constant (including zero) parameters well with minimal error. Table 1 compares the average RMS error for our method with the conventional sliding window approach for multiple samples of small randomly generated networks of different sizes. It can be noted that our proposed tracking scheme consistently outperforms by always producing lower RMSE.

#### 4. EXPERIMENTAL DATA

BOLD time-series data from subjects in a resting state is obtained for five regions of interest (ROIs) corresponding to motor function, a Siemens Trio 3T scanner. Their abbreviations and MNI (Montreal Neurological Institute) coordinates are given in Table 2. Preprocessing involves slice time/motion corrections, normalization, 8-mm smoothing kernel, and low-pass filtering (0.009 – 0.08 Hz).

Our algorithm is applied on a selected data set whose tracking results are displayed in Figure 3. Strong interaction is observed between nodes 1 and 3, and 2 and 3 as expected, as they are known to have strong functional connectivity[26]. Changes in interaction strengths are seen which may correspond to different mind states of the subject during data acquisition. This dynamic response merits further investigation and opens avenues for comparing with networks arising during task-based experiments as well as contrasting network information from healthy volunteers and patients.

Next, data from 22 subjects is analyzed and the mean values obtained for all links are shown in Table 3. As expected, the computed interaction between left pre and post central gyrus is much stronger than between left and right gyrus, and Vermis lobule is very weakly connected to the left gyrus.

Table 2: Five ROIs of motor function and their co-ordinates

ROI	Abbreviation	ROI Area	MNI Coordinates
1	PreCG_L	Left pre-central gyrus	[-36, -22, 64]
2	PreCG_R	Right pre-central gyrus	[60, 8, 28]
3	PoCG_L	Left post-central gyrus	[-40, -26, 52]
4	Ver_6	Vermis lobule 6	[6, -62, 20]

Table 3: Mean values of interaction parameters

Interaction parameter	Mean value
$\varphi_{12}$	-0.21
$\varphi_{13}$	1.09
$\varphi_{14}$	0.09
$\varphi_{23}$	0.29
$\varphi_{24}$	0.39
$\varphi_{34}$	0.08

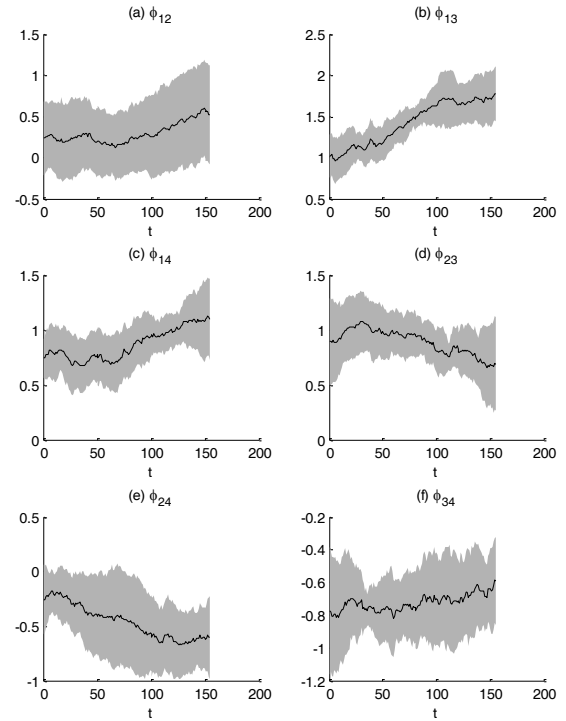


Figure 3: Tracking results from real data. Black line shows estimated mean and grey region shows 1 standard deviation.

#### 5. DISCUSSION

Our work supports the existence of fluctuations in functional connectivity during resting-state and presents an applicable and workable methodology to infer these changes. We aim to extend our work to larger networks covering more areas of the brain as well as infer sparsity in these networks. By employing this method within a Particle-MCMC framework[27], ‘exact’ Monte-Carlo samples could be drawn from  $p(\phi_{1:T}|Z_{1:T})$ , hence resulting in more accurate inference, particularly in early periods. Concurrent studies could be carried out by obtaining independent data using other modalities like EEG in order to verify and complement the information obtained by this fMRI analysis.

In order to gain a better insight into dynamics that underlie neuronal activity networks, this analysis would be further developed to include hemodynamic response such as the non-linear Balloon Model[28][29]. In this way, biologically relevant information about effective connectivity could be obtained. This work has the potential to allow deeper understanding of brain function by allowing the study of dynamic brain states. Disorders such as schizophrenia, depression and Alzheimer’s have been found to alter brain dynamics [16]. Further studies with groups of healthy controls and patients are needed to ascertain potential benefits.

## REFERENCES

- [1] S. M. Smith, K. L. Miller, S. Moeller, J. Xu, E. J. Auerbach, M. W. Woolrich, C. F. Beckmann, M. Jenkinson, J. Andersson, M. F. Glasser, D. C. Van Essen, D. a Feinberg, E. S. Yacoub, and K. Ugurbil, "Temporally-independent functional modes of spontaneous brain activity.," *Proc. Natl. Acad. Sci. U. S. A.*, vol. 109, no. 8, pp. 3131–6, Feb. 2012.
- [2] A. Fornito and E. T. Bullmore, "Connectomics: A new paradigm for understanding brain disease.," *Eur. Neuropsychopharmacol.*, Mar. 2014.
- [3] O. Sporns, "The human connectome: a complex network.," *Ann. N. Y. Acad. Sci.*, vol. 1224, pp. 109–25, Apr. 2011.
- [4] R. Salvador, a Martínez, E. Pomarol-Clotet, S. Sarró, J. Suckling, and E. Bullmore, "Frequency based mutual information measures between clusters of brain regions in functional magnetic resonance imaging.," *Neuroimage*, vol. 35, no. 1, pp. 83–8, Mar. 2007.
- [5] E. Bullmore and O. Sporns, "Complex brain networks: graph theoretical analysis of structural and functional systems.," *Nat. Rev. Neurosci.*, vol. 10, no. 3, pp. 186–98, Mar. 2009.
- [6] C. F. Beckmann, "Modelling with independent components.," *Neuroimage*, vol. 62, no. 2, pp. 891–901, Aug. 2012.
- [7] A. R. McIntosh, "Structural Equation Modeling and Its Application to Network Analysis in Functional Brain Imaging," vol. 22, pp. 2–22, 1994.
- [8] B. Li, J. Daunizeau, K. E. Stephan, W. Penny, D. Hu, and K. Friston, "Generalised filtering and stochastic DCM for fMRI.," *Neuroimage*, vol. 58, no. 2, pp. 442–57, Oct. 2011.
- [9] M. L. Seghier and K. J. Friston, "Network discovery with large DCMs.," *Neuroimage*, vol. 68, pp. 181–91, Mar. 2013.
- [10] K. J. Friston, L. Harrison, and W. Penny, "Dynamic causal modelling.," *Neuroimage*, vol. 19, no. 4, pp. 1273–1302, Aug. 2003.
- [11] K. E. Stephan, L. Kasper, L. M. Harrison, J. Daunizeau, H. E. M. den Ouden, M. Breakspear, and K. J. Friston, "Nonlinear dynamic causal models for fMRI.," *Neuroimage*, vol. 42, no. 2, pp. 649–62, Aug. 2008.
- [12] K. J. Friston, N. Trujillo-Barreto, and J. Daunizeau, "DEM: a variational treatment of dynamic systems.," *Neuroimage*, vol. 41, no. 3, pp. 849–85, Jul. 2008.
- [13] J. Daunizeau, K. J. Friston, and S. J. Kiebel, "Variational Bayesian identification and prediction of stochastic nonlinear dynamic causal models.," *Physica D.*, vol. 238, no. 21, pp. 2089–2118, Nov. 2009.
- [14] L. K. H. Daniel J. Jacobsen, Kristoffer Hougaard Madsen, "Identification of Non-Linear Models of Neural Activity in BOLD fMRI," *IEEE*, pp. 952–955, 2006.
- [15] L. a Johnston, E. Duff, I. Mareels, and G. F. Egan, "Nonlinear estimation of the BOLD signal.," *Neuroimage*, vol. 40, no. 2, pp. 504–14, Apr. 2008.
- [16] R. M. Hutchison, T. Womelsdorf, E. a Allen, P. a Bandettini, V. D. Calhoun, M. Corbetta, S. Della Penna, J. H. Duyn, G. H. Glover, J. Gonzalez-Castillo, D. a Handwerker, S. Keilholz, V. Kiviniemi, D. a Leopold, F. de Pasquale, O. Sporns, M. Walter, and C. Chang, "Dynamic functional connectivity: promise, issues, and interpretations.," *Neuroimage*, vol. 80, pp. 360–78, Oct. 2013.
- [17] R. M. Hutchison, T. Womelsdorf, J. S. Gati, S. Everling, and R. S. Menon, "Resting-state networks show dynamic functional connectivity in awake humans and anesthetized macaques.," *Hum. Brain Mapp.*, vol. 34, no. 9, pp. 2154–77, Sep. 2013.
- [18] U. Sakoglu, G. D. Pearlson, K. a Kiehl, Y. M. Wang, A. M. Michael, and V. D. Calhoun, "A method for evaluating dynamic functional network connectivity and task-modulation: application to schizophrenia.," *MAGMA*, vol. 23, no. 5–6, pp. 351–66, Dec. 2010.
- [19] D. a Handwerker, V. Roopchansingh, J. Gonzalez-Castillo, and P. a Bandettini, "Periodic changes in fMRI connectivity.," *Neuroimage*, vol. 63, no. 3, pp. 1712–9, Nov. 2012.
- [20] E. a Allen, E. Damaraju, S. M. Plis, E. B. Erhardt, T. Eichele, and V. D. Calhoun, "Tracking whole-brain connectivity dynamics in the resting state.," *Cereb. Cortex*, vol. 24, no. 3, pp. 663–76, Mar. 2014.
- [21] S. M. Smith, D. Vidaurre, C. F. Beckmann, M. F. Glasser, M. Jenkinson, K. L. Miller, T. E. Nichols, E. C. Robinson, G. Salimi-Khorshidi, M. W. Woolrich, D. M. Barch, K. Ugurbil, and D. C. Van Essen, "Functional connectomics from resting-state fMRI.," *Trends Cogn. Sci.*, vol. 17, no. 12, pp. 666–82, Dec. 2013.
- [22] G. Deco and M. Corbetta, "The dynamical balance of the brain at rest.," *Neuroscientist*, vol. 17, no. 1, pp. 107–23, Feb. 2011.
- [23] M. W. Woolrich and K. E. Stephan, "Biophysical network models and the human connectome.," *Neuroimage*, vol. 80, pp. 330–8, Oct. 2013.
- [24] S. K. Pang, J. Li, and S. J. Godsill, "Detection and Tracking of Coordinated Groups," *IEEE Trans. Aerosp. Electron. Syst.*, vol. 47, no. 1, pp. 472–502, Jan. 2011.
- [25] O. Cappe, S. J. Godsill, and E. Moulines, "An Overview of Existing Methods and Recent Advances in Sequential Monte Carlo," *Proc. IEEE*, vol. 95, no. 5, pp. 899–924, May 2007.
- [26] M. Kasahara, D. K. Menon, C. H. Salmond, J. G. Outtrim, J. V Taylor Tavares, T. a Carpenter, J. D. Pickard, B. J. Sahakian, and E. a Stamatakis, "Altered functional connectivity in the motor network after traumatic brain injury.," *Neurology*, vol. 75, no. 2, pp. 168–76, Jul. 2010.
- [27] C. Andrieu, A. Doucet, and R. Holenstein, "Particle Markov chain Monte Carlo methods," *J. R. Stat. Soc. Ser. B (Statistical Methodol.)*, vol. 72, no. 3, pp. 269–342, Jun. 2010.
- [28] K. J. Friston, a Mechelli, R. Turner, and C. J. Price, "Nonlinear responses in fMRI: the Balloon model, Volterra kernels, and other hemodynamics.," *Neuroimage*, vol. 12, no. 4, pp. 466–77, Oct. 2000.
- [29] K. E. Stephan, N. Weiskopf, P. M. Drysdale, P. a Robinson, and K. J. Friston, "Comparing hemodynamic models with DCM.," *Neuroimage*, vol. 38, no. 3, pp. 387–401, Nov. 2007.